Applied Catalysis B: Environmental 92 (2009) 61–67

Contents lists available at ScienceDirect

Applied Catalysis B: Environmental

journal homepage: www.elsevier.com/locate/apcatb

Hierarchical mesoporous phosphorus and nitrogen doped titania materials: Synthesis, characterization and visible-light photocatalytic activity

Gao-Song Shao [a], Feng-Yun Wang [a], Tie-Zhen Ren [b], Yuping Liu [a], Zhong-Yong Yuan [a,*]

[a] Institute of New Catalytic Materials Science, Engineering Research Center of Energy Storage and Conversion (Ministry of Education), College of Chemistry, Nankai University, Tianjin 300071, PR China
[b] School of Chemical Engineering & Technology, Hebei University of Technology, Tianjin 300130, PR China

ARTICLE INFO

Article history:
Received 29 April 2009
Received in revised form 7 July 2009
Accepted 20 July 2009
Available online 28 July 2009

Keywords:
Mesoporous
Titania
Phosphorus
Nitrogen
Photoactivity

ABSTRACT

Hierarchical mesoporous P- and N-doped titanias were synthesized by the direct phosphation from phosphoric acid and the following nitridation with urea solution. The resulting materials were characterized by XRD, nitrogen adsorption, SEM, TEM, UV–vis, FT-IR and XPS analysis, and their photocatalytic activities were tested by the visible-light photodegradation of Rhodamine B solution. A bimodal mesopore size distribution with a macroporous structure was observed, rendering high surface area with thermal stability. N-doping of the hierarchical mesoporous titania resulted in the band-gap narrowing with improved photocatalytic activity. However, the phosphated titania exhibited higher photocatalytic activity than the N-doped one, but with larger band-gap energy. Further nitridation of phosphated titania resulted in narrower band-gap of the N,P-codoped titania than either N- or P-doped one, exhibiting the further enhanced photocatalytic activity.

1. Introduction

Visible-light photocatalysis has attracted intense interest because of its potential in utilization of solar energy recently. Many efforts have been devoted to the exploration of semiconductor photocatalytic materials with high catalytic activity and efficient solar energy utilization. Doping of TiO_2 with either anion [1–7] or cation [8–12] or codoping with different dopant [13–15] was found to be an effective method to achieve efficient photocatalysts in the visible-light range. Asahi et al. [2] reported that substitutional doping TiO_2 with nitrogen could narrow its band-gap by mixing of N 2p and O 2p states in the valence band and consequently induce the absorption edge red-shifted to lower energies (longer wavelengths, especially in the visible region), enhancing its visible-light responsive photocatalytic activity. Some studies [16,17] however proposed the appearance of intragap localized N 2p states, related to the photothreshold energy decrease, facilitating the formation of oxygen vacancies. Similar debate of substitutional or interstitial type doping of titania was also found for other dopants, such as carbon [18,19] and sulfur [5,20].

It is reported that the phosphate-modification of titania can result in the improvement of its thermal stability and photocatalytic activity [21–24]. Previous reports by Yu et al. [21], Körösi et al. [22] and Colón et al. [25] demonstrated that the adsorption edge of the phosphate-modified titanias blue-shifted to shorter wavelength, giving higher band-gap energies than pure titania. In contrast, Lin et al. [24] reported the band-gap narrowing in their synthesized P-doped TiO_2, offering an excellent photocatalytic activity in visible light. Thus, it is still necessary to further investigate the mechanism of the nonmetal-doping and the causes for the red-shift or blue-shift of the adsorption edge.

Nanocrystalline titania with mesoporous structure would exhibit a great potential in improving photocatalytic activity because of its abundant pores and large surface area. The incorporation of light-harvesting macroporous channels into a mesoporous titania framework was found to further increase its photocatalytic activity [26,27]. Our previous work [28] demonstrated that the N-doping of hierarchical meso-/macroporous titania material extended effectively its photocatalytic performance into the visible-light region with increased activity. In this paper, we report hierarchical mesoporous phosphorus and nitrogen doped titanias as active visible-light photocatalysts by a simple template-free synthesis route. *n*-propanol was added in the hydrolyzation process of titanium alkoxide, in order to optimize the mesoporous structure, and the synthesized phosphorus and nitrogen codoped mesoporous titania exhibited better photocatalytic activity in visible light than either phosphorus or nitrogen doped one. The effect of two dopants on the physicochemical properties of the resultant doped mesoporous titanias, as

* Corresponding author. Tel.: +86 22 23509610; fax: +86 22 23509610.
E-mail address: zyyuan@nankai.edu.cn (Z.-Y. Yuan).

0926-3373/$ – see front matter © 2009 Elsevier B.V. All rights reserved.
doi:10.1016/j.apcatb.2009.07.024

well as on the photocatalytic activity for photodegradation of Rhodamine B (RhB) under visible light, was investigated.

2. Experimental

2.1. Catalyst preparation

All chemicals were used as received, without further purification. In order to reduce the speed of the titanium *n*-alkoxide hydrolyzation, we dilute the concentration of *n*-tetrabutyl titanate (Kermel, AR) by adding *n*-propanol solution with a *n*-tetrabutyl titanate/*n*-propanol molar ratio of 4.9. 8.7 g of the mixture of tetrabutyl titanate and *n*-propanol was dropwise added into 30 mL of phosphoric acid solution (pH 2) and slowly stirred at room temperature until the titanium *n*-alkoxide hydrolyzed completely. The mixture was transferred into a Teflon-lined autoclave and heated statically in an oven at 60 °C for two days. The solid was then filtered, washed and dried, which was denoted as MTP. The mesoporous pure titania (MT) was obtained by hydrolyzation of pre-treated tetrabutyl titanate/*n*-propanol mixed solution in the deionized water. The calcined products of MT and MTP at 450 °C for 2 h were denoted as MT450 and MTP450 respectively.

To further perform nitrogen-doping, 2 g of the obtained MT or MTP powder was mixed with 5 mL of urea aqueous solution (2 mol/L), and slowly magnetically stirred at room temperature for 5 h. The mixture was kept at room temperature for 48 h, and then washed with very dilute sulfuric acid and deionized water, and dried at 60 °C in air. Finally the resultant white powder was calcined at 450 °C for 2 h, and denoted as MTN or MTPN respectively.

2.2. Sample characterization

X-ray diffraction (XRD) patterns were collected on a Rigaku D/max-2500 diffractometer with Cu Kα radiation operated at 40 kV and 100 mA.

N_2 adsorption–desorption isotherms were recorded on a Quantachrome NOVA 2000e sorption analyzer at liquid nitrogen temperature (77 K). The samples were degassed at 200 °C overnight prior to the measurement. The surface area was obtained by the Brunauer–Emmett–Teller (BET) method, and pore size distribution was calculated from the adsorption branch of the isotherm by the Barret–Joyner–Halenda (BJH) model or non-local density functional theory (NLDFT) method.

Scanning electron microscopy (SEM) was taken on a Shimadzu SS-550 microscope at 15 keV. Transmission electron microscopy (TEM) was carried out on a Philips Tecnai G20 microscope, working at 200 kV. A trace amount of sample was dispersed in ethanol solution by sonication for 10 min, and then deposited on a carbon-coated copper grid, which was used as a TEM specimen.

Fourier transform infrared (FT-IR) spectroscopy was carried out on a Bruker VECTOR 22 spectrometer, with KBr pellet technique.

UV–vis absorption spectroscopy was employed on a JASCO V-570 UV-V-NIR spectrophotometer over the wavelength range 300–1000 nm, using $BaSO_4$ as a reference.

X-ray photoelectron spectroscopy (XPS) measurements were performed on a Kratos Axis Ultra DLD (delay line detector) spectrometer equipped with a monochromatic Al Kα X-ray source (1486.6 eV). All XPS spectra were recorded using an aperture slot of 300 μm × 700 μm, survey spectra were recorded with a pass energy of 160 eV, and high-resolution spectra with a pass energy of 40 eV.

2.3. Measurement of photocatalytic activity

The photocatalytic activity of the prepared catalysts was evaluated by the degradation of Rhodamine B (RhB) dye under visible-light irradiation. 20 mg of the catalyst powder was placed into a tubular quartz reactor of 100 mL of RhB aqueous solution (1×10^{-5} mol/L, pH 6), and a 40-W tungsten bulb was used as the visible-light region source, of which the wavelength range is usually considered as 400–2500 nm, located at 10 cm higher than the solution surrounded by a circulating water tube. All runs were conducted at ambient pressure and temperature. The suspensions were magnetically stirred in the dark for 30 min to ensure the establishment of an adsorption/desorption equilibrium, and then exposed to the light irradiation at room temperature. At given time intervals, about 5 mL of liquor was sampled, centrifuged for 5 min to discard any sediment. The absorbance of reaction solutions was measured using a SP-722 spectrometer at λ_{max} = 554 nm for RhB dye.

3. Results and discussion

3.1. Crystal structure, morphology and porosity

The controlled hydrolysis of the titanium alkoxide solution in water or phosphoric acid solution resulted in the formation of hierarchical mesoporous titania (MT) or phosphated titania (MTP), respectively, which could be transformed into hierarchical mesoporous N-doped titania (MTN) or P,N-codoped titania (MTPN) after nitridation. XRD was performed to investigate the structural phases and crystallite sizes of the samples (Fig. 1). The sample MT presents a main phase of anatase with trace amount of brookite, but pure anatase phase was found in the sample MTP with the lower intensity of (1 0 1) peak located at 2θ = 25.2–25.3° of anatase than MT, suggesting that the direct phosphation prevented the formation of phase impurity. After nitridation, the intensities of diffraction peaks of both pure titania and phosphated titania increased, indicating the crystallization of titania particles during calcination treatment of nitridation process. The calcination of MT and MTP at the nitridation temperature of 450 °C resulted in no changes of structural phases except slight increase in diffraction intensities due to the recrystallization effect. A rough estimation of the crystallite size using the Scherrer–Debye formula is listed in Table 1, based on the strongest peak (1 0 1) of anatase. It is seen that the average crystallite sizes of MTP and MTPN are slightly smaller than that of the samples MT and MTN, which is same as the results previously reported by Shi et al. [23] and Lin et al. [24], indicating that the doping of phosphorus could efficiently inhibit the grain growth.

The N_2 adsorption–desorption isotherms of the synthesized samples and their corresponding pore size distributions are shown in Fig. 2. The isotherms recorded for MT and MTP materials correspond to Type II isotherms with the appearance of the capillary

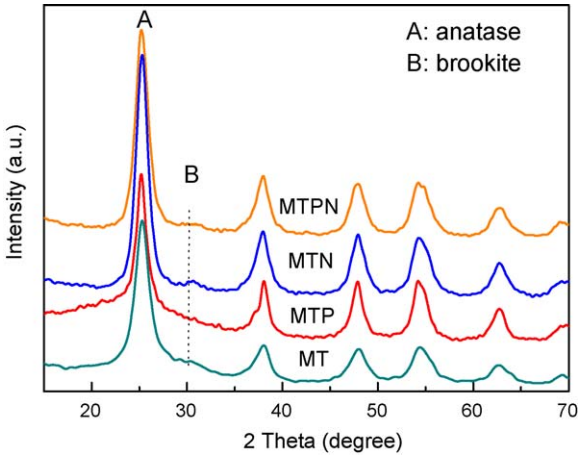

Fig. 1. XRD patterns of prepared samples.

Table 1
Summary of the textural properties, band-gap energies and the photodegradation rate constants of the synthesized samples.

Samples	Crystallite size[a] (nm)	S_{BET}[b] (m^2/g)	D_{ads}[c] (nm)	D_{ave}[d] (nm)	V_{pore}[e] (cm^3/g)	Content by XPS (%)		Band-gap (eV)		Degradation rate of RhB, k (min^{-1})
						N	P	E_{g1}	E_{g2}	
MT	6.1	202	5.1	4.4	0.22	–		3.2	–	1.1×10^{-3}
MT450	7.9	159	5.5	4.6	0.20	–				9.3×10^{-4}
MTP	5.3	272	5.5	5.1	0.35	–		3.32	–	3.0×10^{-3}
MTP450	5.5	246	5.6	5.3	0.34	–				2.7×10^{-3}
MTN	7.3	183	5.3	4.5	0.21	0.92	–	3.22	2.58	2.0×10^{-3}
MTPN	5.8	239	5.7	5.5	0.33	0.68	3.46	3.22	2.44	4.9×10^{-3}

[a] Calculated by the Scherrer formula.
[b] BET surface area calculated from the linear part of the BET plot.
[c] Estimated using the adsorption branch of the isotherm based on the NLDFT mode.
[d] Average pore size calculated by the formula $D = 4V/A$, where A is surface area, V is the pore volume.
[e] Single point total pore volume of pores at $P/P_0 = 0.98$.

condensation, which showed a gradual increase in the amount adsorbed with the relative pressure, suggesting the adsorption on macroporous solids via multilayer formation. A hysteresis loop of Type H3 was observed in the isotherms of these two samples, suggesting the materials with slit-like pores due to the particle aggregation or assembly [29]. The similar adsorption isotherms were also observed by Yu et al. [21] in their phosphated mesoporous titanium dioxides, though they are regarded as Type IV isotherms for mesoporous materials. As to the nitridation products, the samples MTN and MTPN exhibited Type IV isotherms with Type H2 hysteresis loops, suggesting the presence of mesopores with narrow mouths (ink-bottles-like pores) [29]. The type difference of isotherms after nitridation maybe resulted from the growth of the crystallites and the collapse of macroporous framework during nitrogen-doping under high-temperature. The pore size distribution curves, calculated by the NLDFT model, show bimodal distributions at 3–4 nm and 5–6 nm for all samples. The textural properties of the samples are listed in Table 1. It is seen that the synthesized MT has smaller pore size with lower surface area than the sample MTP, indicating the effect of phosphation. And their nitridation products MTN and MTPN give enlarged pore sizes with the decrease in their surface areas and pore volumes (Table 1), due to the effect of the heating treatment. In our previous work [28], the surface area of the mesoporous/macroporous titania synthesized without the use of *n*-propanol decreased from 280 to 121 m^2/g after the same nitridation process, however in this work, only 19 m^2/g of surface area loss was observed for MTN. Also the phosphated samples (MTP and MTPN) possess higher surface areas than non-phosphated samples, revealing that adding *n*-propanol in the synthesis process and/or phosphation can efficiently enhance the thermal stability of the resultant materials. It is also seen that the extent of the surface area decrease and pore size enlargement in the phosphated and calcined/nitrided samples MTP450 and MTPN are less than the non-phosphated ones MT450 and MTN (Table 1).

Fig. 3 shows the representative SEM and TEM images of samples MTP and MTPN. The sample MTP (Fig. 3a) exhibits one macroscopic network structure with relatively homogeneous macropores of ~1 μm in size, accompanying some small holes in the macroporous walls due to the nanoparticle assembly, which has been reflected in the nitrogen adsorption–desorption isotherms. The sample MT has the similar macroporous morphology, and the formation of such a macroporous structure should follow a spontaneous self-assembly formation mechanism as described previously [27,28,30]. After nitridation, the macroporosity diminished for both MTN and MTPN. As seen in Fig. 3b–d, the well-defined macroporous structure was damaged in some of MTPN monoliths, instead of the aggregation of small MTPN grains, leaving a lot of interparticle voids. In the retained monoliths of macroporous structure, the macroporous walls between macrochannels were solidified, dissolving the small holes that were

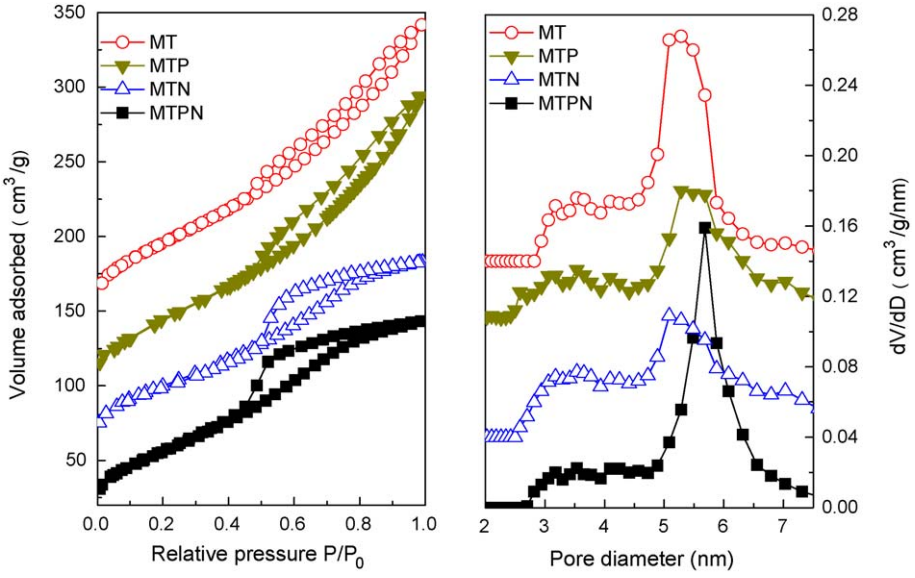

Fig. 2. (Left) N_2 adsorption–desorption isotherms of the prepared samples and (right) the corresponding pore size distribution curves based on the NLDFT model. The volume was shifted by 50, 70 and 130 respectively and the dV/dD value was shifted by 0.04, 0.10 and 0.14 respectively for the curves of samples MTN, MTP and MT.

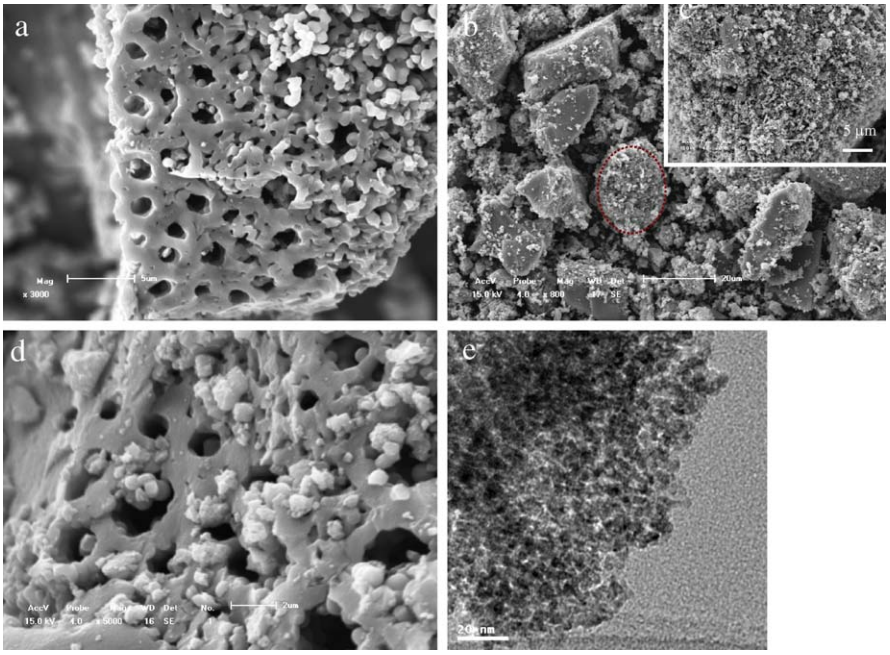

Fig. 3. (a) SEM image of sample MTP; (b–d) SEM and (e) TEM images of sample MTPN. (c) is high-magnification image of (b) (select region in circle).

observed in the samples before nitridation. This morphological difference between the samples before and after nitridation is mainly due to the result of high-temperature treatment during nitrogen-doping. TEM images (Fig. 3e) reveal the wormhole-like mesopores, resulted from the assembly of nanoparticles sized tens of nanometers, in the macroporous walls of the samples both before and after nitridation.

3.2. Chemical structure characterization

In order to verify the elements in the valence and bonding of materials, the FT-IR and XPS spectroscopy were carried out. The FT-IR spectra of the prepared samples in the 400–4000 cm^{-1} range are shown in Fig. 4. The broad absorption bands around 3400 cm^{-1} and the bands at 1630 cm^{-1} correspond to the surface-adsorbed water and the hydroxyl groups [31], and their intensities of the sample MTPN are stronger than that of phosphorus-free samples MT and MTN, suggesting more surface-adsorbed water and hydroxyl groups on the surfaces of nitrogen and phosphorus codoped titanias. The number of a specific anatase Ti–OH group is an important precursor for the reactive site and a dominant factor in controlling performance of photocatalytic degradation. Low-frequency bands in the range <500 cm^{-1} correspond to the Ti–O–Ti vibration of the network [32]. One strong band at $\sim$1034 cm^{-1} is obviously observed in the FT-IR spectra of MTPN and MTP samples, but is absent in the samples without phosphorus-doping (MT and MTN). This band is often characteristic of PO_4^{3-} [33,34], and can also be attributed to the formation of Ti–O–P bond [34,35]. Bhaumik and Inagaki [34] believed that the peaks appearing at 1000–1050 cm^{-1} could result from Ti–O–P framework vibrations. Vasylyev et al. [35] observed a new band at 1026 cm^{-1} in the FT-IR spectrum of titanium phosphonate porous materials constructed from dendritic tetraphosphonates, and assigned it to P–O···Ti vibrations. However, another characteristic frequency of PO_4^{3-}, the P=O (phosphoryl groups) peak at 1300–1450 cm^{-1} [24] is absent in the spectra of MT and MTN samples, but present in the samples MTP and MTPN. It is interesting that the intensity of MTP at this frequency is stronger than MTPN, while that of the band at $\sim$1034 cm^{-1} is opposite, which may suggest that P species in MTP mainly stayed on the surface, but during the following nitridation (i.e. heat-treatment) process, trace amounts of P could diffuse into the bulk titania to form new bonds. The additional peaks at $\sim$1403 and $\sim$1467 cm^{-1}, observed in the spectra of the nitridation samples MTN and MTPN, could be attributed to the nitrogen atoms embedded in the TiO_2 network [36,37] which were not found in the samples MTP and MT. Additionally, an adsorption peak at $\sim$1564 cm^{-1} is observed in the spectra of MTPN, and the peak at this frequency should correspond to the P species and had a shift result from the effect of doped N on P species. Since no peaks appear at 1618, 1318, and 750 cm^{-1}, which are the typical infrared bands of NO_2, there is no possibility for significant formation and/or physical sorption of NO_2 species on the surface of the monitored particles [38].

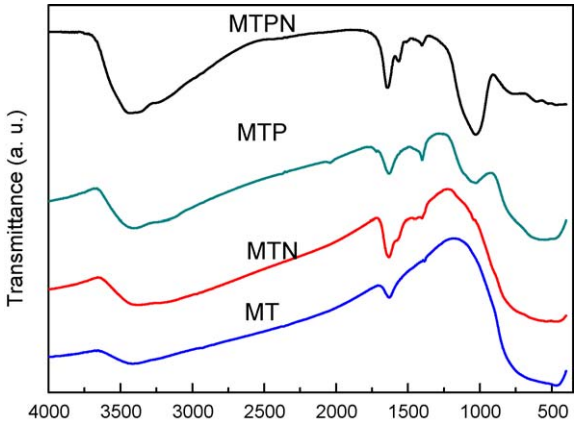

Fig. 4. FT-IR spectra of the synthesized samples.

Fig. 5 shows the high-resolution XPS spectra of Ti 2p, O 1s, N 1s and P 2p taken on the surface of the samples MTN and MTPN. The binding energies of only nitrogen doped titania MTN are situated at 458.0 and 463.7 eV for Ti $2p_{3/2}$ and Ti $2p_{1/2}$ respectively, which are characteristic of Ti^{4+}. Compared with the binding energy of pure titania (459 eV for Ti $2p_{3/2}$ and 464.8 eV for Ti $2p_{1/2}$), the binding energy of Ti 2p decreased after nitrogen-doping. This is the result

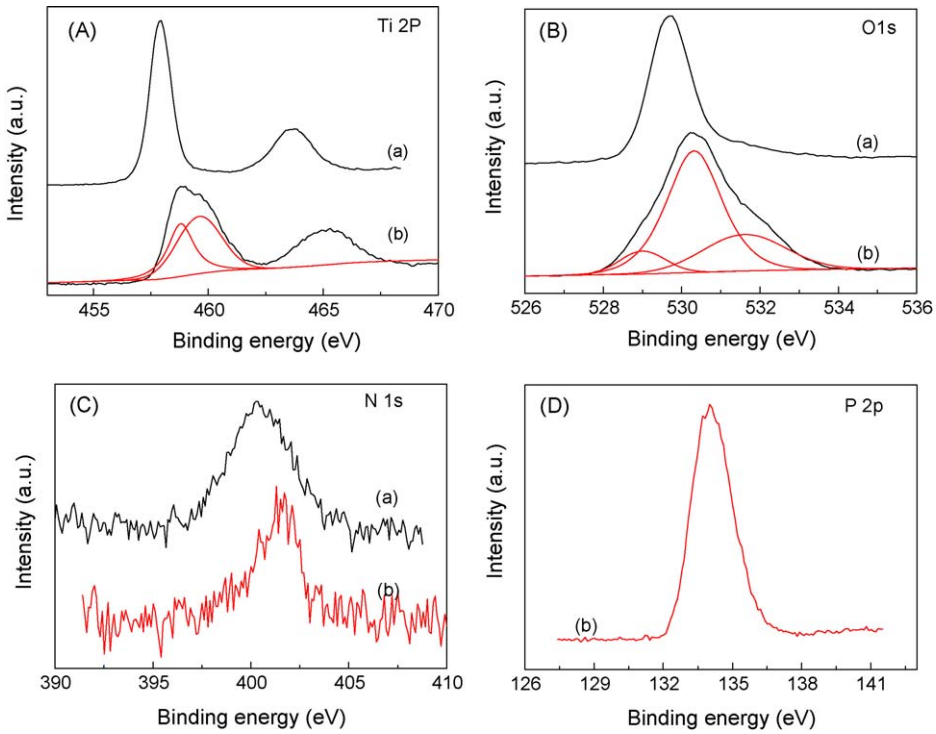

Fig. 5. (A) Ti 2P, (B) O 1s, (C) N 1s, and (D) P 2p XPS spectra of the synthesized samples (a) MTN and (b) MTPN.

from different electronic interactions of Ti with anions, and the same phenomenon has been observed in the previous work on the N-doped titanias [28]. While for Ti 2p in MTPN, the Ti $2p_{1/2}$ peak at 465.2 eV, and the broad Ti $2P_{3/2}$ consists of two peaks at 458.8 and 459.6 eV with an atomic ratio of about 17–25, respectively. This implies that two different chemical environments of Ti ions exist in the MTPN structure. The first Ti ions can be assigned to an octahedral coordination with oxygen, and the second Ti ions are in a tetrahedral environment [39,40]. Ti ions in a tetrahedral coordination are more effective in adsorbing water [21,41], which is already confirmed by the FT-IR result. The binding energy of sample MTPN did not further shift towards lower binding energy as the case of nitrogen-doping, but shifted to opposite direction, suggesting the effect of phosphorus-doping.

The O 1s signal of sample MTN presents one single peak at 529.7 eV (Fig. 5B), which is ascribed to the oxygen in Ti–O bond of TiO_2. The O 1s region of the sample MTPN can be fitted as three peaks: the main peak at the binding energy of 530.0 eV with 67.24% in contribution is the Ti–O bonds in TiO_2, the binding energy of the P–O at 531.0 eV, and the hydroxyl groups or the C–O bond at the binding energy around 532 eV.

The N 1s spectrum of MTN shows one broad peak at 400.3 eV, while MTPN at 401.5 eV (Fig. 5C). Although the assignment of the XPS peak of N 1s has been under debate for a long time, the N 1s spectra of our samples are observed in the range of previously reported nitrogen doped titanias [42–45], which are higher than that of TiN appeared at $\leq$397.5 eV [46], and lower than that of hyponitrite type nitrogen at 404 eV. The peaks of 400.3–401.5 eV might be ascribed to the anionic N^- in O–Ti–N linkages [38,47–49], though this line was attributed to adsorbed molecular nitrogen in some literature. Compared with the spectrum of MTN, a positive shift of 1.2 eV was observed for the sample MTPN, suggesting the effect of P-doping. The shift to a higher binding energy indicates a decrease in the electron density of the N atom. Indeed, the peak at 401.5 eV could not only be attributed to the nitrogen substitute oxygen in form of O–Ti–N [38,47–49], but also be assigned to the phosphorus substitute titanium in form of O–P–N [47]. That is to say, some N atoms coordinated to P in the form of O–P–N linkage for the MTPN sample [47].

The P 2p binding energy of MTPN is observed at 133.7 eV (Fig. 5D), suggesting that phosphorus in the sample MTPN exists in a pentavalent-oxidation state (P^{5+}) [50], and no peak observed at 128.6 eV that was the characteristic binding energy of P 2p in TiP [51], indicating the absence of Ti–P bonds in MTPN. Since the ionic radii of Ti^{4+} and P^{5+} are 0.67 and 0.38 Å (in an environment of coordination number 6) [52], respectively, from the view of radius matching, it is suggested that P atoms were probably incorporated as cations and replaced Ti ions in the crystal lattice of titania, like S^{6+} [5,20] and I^{5+} [7] doped TiO_2 crystal lattice in the form of Ti–O–P bonds [53]. The replacement of a part of Ti^{4+} in TiO_2 lattice by P^{5+} would result in charge imbalance [23,24], and decrease the recombination rate of photogenerated electrons and holes. Furthermore, the valence state of doped P (+5) is higher than that of Ti (+4), which would result in a decrease in outer electron density of the Ti atom in the form of Ti–O–P, and this should be the reason for the increase in Ti 2p binding energy. Therefore, based from the FT-IR and XPS analysis, it is believed that N and P atoms were probably incorporated as anions and cations in the crystal lattice of TiO_2, replacing O and Ti, respectively. The surface atomic compositions of MTN and MTPN determined by the XPS results are listed in Table 1. It is seen that the content of P is relatively large, and the content of N in MTPN is less than that in MTN. This indicates that N atoms were a little difficult when incorporating into the crystal lattice of phosphated TiO_2. A small part of P atoms might be in the form of amorphous titanium phosphate species embedded in the TiO_2 crystallites, in agreement with the XRD, FT-IR and XPS analysis.

3.3. Optical property

The UV–vis spectra of the samples are shown in Fig. 6. The MT and MTP samples show single sharp edges with the band-gap absorption onset at 387 and 373 nm respectively, while the nitridation samples (MTN and MTPN) exhibit a high tailing absorbance in the longer wavelength (>400 nm), giving two absorption edges, which

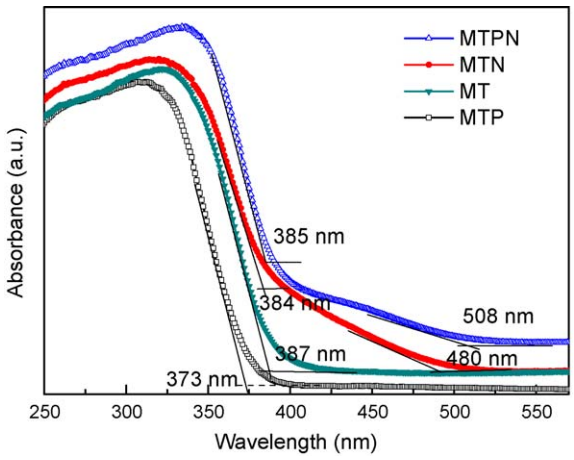

Fig. 6. UV–vis diffuse reflectance spectra of the synthesized samples.

indicates the absorption edge extending into the visible region. The band-gap energies (E_g) were calculated by the formula $E_g = 1239.8/\lambda_g$ from the wavelength values corresponding to the intersection point of the vertical and horizontal parts of the spectra (λ_g), and the corresponding band-gaps are listed in Table 1. The UV–vis spectra of MTN and MTPN are red-shifted in comparison with that of MT, with the narrowing of their band-gaps, as the previously reported nitrogen doped titanias [2,16,17,28,37,54], demonstrating that they are sensitive to visible light. In contrast, the UV–vis spectrum of MTP is blue-shifted, and its band-gap is larger than that of MT, different from the case of nitrogen-doping. A similar blue-shift was observed in the case of phosphoric acid pre-treatment of titania by Yu et al. [21] and Körösi et al. [22,55], and the higher band-gap energy after phosphoric acid treatment on titania was partly accounted for the change in the structure of the titanium dioxide surface (chemisorbed phosphate and trace amorphous titanium phosphate) and partly for the smaller particle size of titania (quantum-size effect) [22]. This is different to the case of Lin et al. [24] and Shi et al. [23] in that the red-shift of the absorbance edge to the visible region was observed in their P-doped titanias with reduced band-gap energy, which may be probably due to the differences in preparation techniques and the difference in the phosphate contents. Yang et al. [56] believed that the band-gap of P cation-doped anatase had few modifications and no impurity energy levels by their electronic structure calculations, favoring the recent observations that the higher photocatalytic activity in P cation-doped TiO_2 resulted from the large surface area and the crystallinity of TiO_2 rather than the formation of an impurity energy level within the band-gap [21]. Since the energy gaps in the porous titanium phosphates were ca. 3.8 eV estimated from the adsorption edge (330 nm) [34], which was larger than that of TiO_2 (ca. 3.0 eV), the presence of trace of amorphous titanium phosphate species embedded in the mesoporous TiO_2 crystallites may account for the blue-shift in UV–vis spectrum of the MTP sample. The FT-IR and XPS spectra of our samples have also revealed the presence of Ti ions in both tetrahedral and octahedral coordination in the P-doped titanias, and more hydroxide groups on the surface of MTP than that of MT, which can act as Lewis acid sites to easily adsorb oxygen and water molecules, possibly corresponding to a more powerful redox ability for photocatalytic reaction.

Although the absorption edge blue-shifted in the MTP and red-shifted in the MTN in comparison with MT, N- and P-codoped titania (MTPN) has a stronger red-shift than only N-doped titania (MTN). Lin et al. [24] reported the similar extension of the absorbance shoulder towards longer wavelength for their N- and P-codoped titanias. Different chemical structures between MTN and MTPN have been revealed from the XPS and FT-IR spectra, due to the effect of P-doping, resulting in the formation of an impurity energy level within the band-gap of TiO_2. It is estimated that the induced effect of nitrogen-doping allowing sub-band-gap excitation is due to an isolated N 2p state rather than to mixed states of N 2p and O 2p, in good agreement with a few early reports [16,17]. When nitrogen was doped into P-doped titania, the crystallite size enlarged with heavy yellow color, and the chemical states of O 1s, N 1s and Ti 2p were observed, which mainly account for enhanced absorption of visible light. The synergistic reaction of phosphorus and nitrogen could be expected in the sample MTPN for its high absorption in the visible light.

3.4. Photocatalytic activity

The photocatalytic activities of the synthesized hierarchical mesoporous TiO_2 doped with N and P were tested by the degradation of RhB under visible-light irradiation (Fig. 7). For comparison, a blank experiment (self-photosensitized process, in the absence of any catalysts) was performed under identical conditions. The self-degradation process is inactive under visible-light region irradiation, as evidenced by only 1.2% RhB degraded after 100 min irradiation. For the pure titania sample MT, 10.1% of RhB was degraded after 100 min irradiation, while for the N- and P-doped samples MTN, MTP and MTPN, the RhB was degraded 17.9%, 28.7% and 39.7%, respectively, indicating the P- or/and N-doped titanias are active under visible light. The photocatalytic activity of MTN was lower than that of MTP, however, could be further enhanced by codoping with both P and N. The MTPN has the higher photocatalytic activity than the samples doped only N or P, suggesting the synergistic effect of N- and P-codoping.

The photocatalytic degradation reaction can be assumed to follow a pseudo-first-order expression: $\ln(C_0/C) = kt$, where C_0/C is

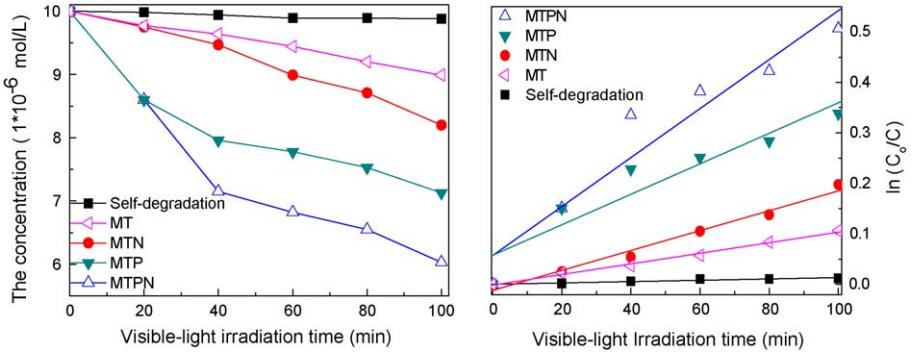

Fig. 7. (Left) The residual organic compounds concentration of solution after photodecomposition by catalysts under visible-light irradiation; (Right) A plot of $\ln(C_0/C)$ versus the irradiation time, showing the fitting results using the pseudo-first-order reaction.

the normalized organic compounds concentration and k is the apparent reaction rate (min^{-1}). The photocatalytic activity has been defined as the overall degradation rate constant of the catalysts. By plotting $\ln(C_0/C)$ as a function of irradiation time through regression (Fig. 7), the k constant from the slopes of the simulated straight lines can be obtained. The calculated k constants are listed in Table 1. The self-degradation rate constant is relatively low ($1.3 \times 10^{-4}\ min^{-1}$). The degradation rate of only $1.1 \times 10^{-3}\ min^{-1}$ is seen for sample MT, even a litter lower degradation rate constant of $9.3 \times 10^{-4}\ min^{-1}$ for its calcined product MT450. The constants k increase as the order of MTN < MTP < MTPN from $2.0 \times 10^{-3}\ min^{-1}$ to $4.9 \times 10^{-3}\ min^{-1}$ (Table 1). In many previous studies [2–20,28,43–46], the band-gap narrowing of the titania-based photocatalysts were always emphasized to correlate the photocatalytic activity. However, in this work, although the band-gap of MTP is larger than that of MT and MTN, its photocatalytic activity is higher, suggesting that one should be careful when evaluating the band-gap values of the photocatalysts with the photocatalytic activities. Yu et al. [21] and Körösi et al. [22] have also observed the enlargement of the band-gap values by the phosphation (or P-doping) of titanias, but giving the enhancement of the photocatalytic activity, which was explained by the increased band-gap energy, large surface area, and the existence of Ti ions in tetrahedral coordination. Colón et al. [25] found that the photoactivity strongly decreased after phosphoric acid treatment, though a similar blue-shift of adsorption edge was observed, which might be determined by the appearance of pyrophosphate-like species at the surface. Zheng et al. [53] also observed no appreciable absorption in visible-light region region in UV–vis spectrum of their visible-light photoactive P-doped titania, but the origin of this phenomenon was not clear. The similar case was also observed in F-doped TiO_2, whose photocatalytic property in visible light was explained by the combined action of lattice and surface F species [57,58].

In our case, high surface area and small crystallite size were obtained in the phosphated titanias (Table 1), which would benefit the increase in the photocatalytic activity of MTP and MTPN. More hydroxyl groups on the surface of P-doped TiO_2 than N-doped TiO_2 were offered as active sites for photocatalytic reaction. Furthermore, phosphate ions incorporated into the surface of titania as amorphous titanium phosphate species, which resulted in the enhancement of the surface area [59], may inhibit the electron–hole recombination due to their ability to trap photogenerated holes, and reactive radicals formed, resulting in improved photocatalytic activity [22]. Further modification of P-doped TiO_2 with nitrogen has a complex effect on the photooxidation, resulting from the cooperation reaction by N- and P-doping, and significant increase in photocatalytic activity was obtained.

4. Conclusions

Hierarchical mesoporous N- and P-doped titania catalysts were prepared by the direct hydrolysis of the mixture of titanium alkoxide and n-propanol, and followed by the nitridation with urea solution at 450 °C. The obtained materials possess a bimodal mesoporous distribution, besides a macroporous structure, having a high surface area with thermal stability. The photocatalytic activity of N-doped titania was lower than that of P-doped titania. The chemical nature of N and P has been well-identified to be N–Ti–O and Ti–O–P in the anatase TiO_2 lattice, and the O–P–N linkage was also in the N,P-codoped titania sample, which showed the highest photocatalytic activity in the N or/and P-doped titania samples. The modulation of the textural and optical properties could be accomplished by the modification with nitrogen and phosphorus, further affecting the photocatalytic activity of the resultant materials. The measured band-gap energy value cannot be regarded as a direct response to the level of photocatalytic activity.

Acknowledgements

This work was supported by the National Natural Science Foundation of China (20473041, 20673060), the National Basic Research Program of China (2009CB623502), the Specialized Research Fund for the Doctoral Program of Higher Education (20070055014), the Natural Science Foundation of Tianjin (08JCZDJC21500), the Chinese-Bulgarian Scientific and Technological Cooperation Project, the Fund from Hebei Provincial Department of Education (2007313), the Program for New Century Excellent Talents in University (NCET-06-0215), and Nankai University.

References

[1] S. Sato, Chem. Phys. Lett. 123 (1986) 126.
[2] R. Asahi, T. Morikawa, T. Ohwaki, K. Aoki, Y. Tage, Science 293 (2001) 269.
[3] S. Sakthivel, H. Kisch, ChemPhysChem 4 (2003) 487.
[4] M. Shen, Z. Wu, H. Huang, Y. Du, P. Yang, Mater. Lett. 60 (2006) 693.
[5] J.C. Yu, W. Ho, J.G. Yu, H. Yip, P.K. Wong, J.C. Zhao, Environ. Sci. Technol. 39 (2005) 1175.
[6] W. Ho, J.C. Yu, S. Lee, Chem. Commun. (2006) 1115.
[7] X.T. Hong, Z.P. Wang, W.M. Cai, F. Lu, J. Zhang, Y.Z. Yang, N. Ma, Y.J. Liu, Chem. Mater. 17 (2005) 1548.
[8] Y. Wang, Z.H. Jiang, F.J. Yang, Mater. Sci. Eng. B 134 (2006) 76.
[9] A. Ghicov, B. Schmidt, J. Kunze, P. Schmuki, Chem. Phys. Lett. 433 (2007) 323.
[10] K. Zhang, W. Xu, X. Li, S. Zheng, G. Xu, Cent. Eur. J. Chem. 4 (2006) 234.
[11] Y.H. Xu, H.R. Chen, Z.X. Zeng, B. Lei, Appl. Surf. Sci. 252 (2006) 8565.
[12] H. Yu, X.J. Li, S.J. Zheng, W. Xu, Mater. Chem. Phys. 97 (2006) 59.
[13] D. Li, H. Haneda, S. Hishita, N. Ohashi, Chem. Mater. 17 (2005) 2588.
[14] H. Sun, Y. Bai, Y. Cheng, W. Jin, N. Xu, Ind. Eng. Chem. Res. 45 (2006) 4971.
[15] D. Chen, Z. Jiang, J. Geng, Q. Wang, D. Yang, Ind. Eng. Chem. Res. 46 (2007) 2741.
[16] H. Irie, Y. Watanabe, K. Hashimoto, J. Phys. Chem. B 107 (2003) 5483.
[17] T. Linsgren, J.M. Mwabora, E. Arendaño, J. Jonsson, A. Hoel, C.-G. Granqvist, S.-E. Lindquist, J. Phys. Chem. B 107 (2003) 5709.
[18] S.U.M. Khan, M. Al-Shahry, W.B. Ingler, Science 297 (2002) 2243.
[19] Y. Li, D.S. Hwang, N.H. Lee, S.J. Kim, Chem. Phys. Lett. 404 (2005) 25.
[20] T. Ohno, T. Mitsui, M. Matsumura, Chem. Lett. 32 (2003) 364.
[21] J.C. Yu, L. Zhang, Z. Zheng, J. Zhao, Chem. Mater. 15 (2003) 2280.
[22] L. Körösi, S. Papp, I. Bertóti, I. Dékány, Chem. Mater. 19 (2007) 4811.
[23] Q. Shi, D. Yang, Z.Y. Jiang, J. Li, J. Mol. Catal. B 43 (2006) 44.
[24] L. Lin, W. Lin, J.L. Xie, Y.X. Zhu, B.Y. Zhao, Y.C. Xie, Appl. Catal. B 75 (2007) 52.
[25] G. Colón, J.M. Sánchez-Espana, M.C. Hidalgo, J.A. Navío, J. Photochem. Photobiol. A 179 (2006) 20.
[26] X.C. Wang, J.C. Yu, C. Ho, Y.D. Hou, X.Z. Fu, Langmuir 21 (2005) 2552.
[27] Z.Y. Yuan, B.L. Su, J. Mater. Chem. 16 (2006) 663.
[28] G.-S. Shao, X.-J. Zhang, Z.-Y. Yuan, Appl. Catal. B 82 (2008) 208.
[29] M. Kruk, M. Jaroniec, Chem. Mater. 13 (2001) 3169.
[30] A. Collins, D. Carriazo, S.A. Davis, S. Mann, Chem. Commun. (2004) 568.
[31] T.Z. Ren, Z.Y. Yuan, B.L. Su, Chem. Phys. Lett. 374 (2003) 170.
[32] G.J. Soler-Illia, A.A.A. Louis, C. Sanchez, Chem. Mater. 14 (2002) 750.
[33] S.K. Samantaray, K. Parida, Appl. Catal. A 220 (2001) 9.
[34] A. Bhaumik, S. Inagaki, J. Am. Chem. Soc. 123 (2001) 691.
[35] M.V. Vasylyev, E.J. Wachtel, R. Popovitz-Biro, R. Neumann, Chem. Eur. J. 12 (2006) 3507.
[36] L.A. Nalo, C.C. Cerrlos, C. Real, J. Surf. Interface Anal. 24 (1996) 355.
[37] H. Li, J. Li, Y. Huo, J. Phys. Chem. B 110 (2006) 1559.
[38] X. Chen, Y. Lou, A.C.S. Samia, C. Burda, J.L. Gole, Adv. Funct. Mater. 15 (2005) 41.
[39] S.M. Mukhopadhyay, S.H. Garofalini, J. Non-Cryst. Solids 126 (1990) 202.
[40] A.A.S. Alfaya, Y. Gushikem, Chem. Mater. 10 (1998) 909.
[41] P. Jones, J.A. Hockey, Trans. Faraday Soc. 67 (1971) 2679.
[42] Y. Cong, J. Zhang, F. Chen, M. Anpo, J. Phys. Chem. C 111 (2007) 6976.
[43] R. Nakamura, T. Tanaka, Y. Nakato, J. Phys. Chem. B 108 (2004) 10617.
[44] J.L. Gole, J.D. Stout, C. Burda, Y. Lou, X. Chen, J. Phys. Chem. B 108 (2004) 1230.
[45] X. Chen, C. Burda, J. Phys. Chem. B 108 (2004) 15446.
[46] N.C. Saha, H.G. Tompkins, J. Appl. Phys. 72 (1992) 3072.
[47] L. Lin, R.Y. Zheng, J.L. Xie, Y.X. Zhu, Y.C. Xie, Appl. Catal. B 76 (2007) 196.
[48] M. Sathish, B. Viswanathan, R.P. Viswanath, C.S. Gopinath, Chem. Mater. 17 (2005) 6349.
[49] T. Ma, M. Akiyama, E. Abe, I. Imai, Nano Lett. 5 (2005) 2543.
[50] S.J. Splinter, R. Rofagha, N.S. Mcintyre, U. Erb, Surf. Interface Anal. 24 (1996) 81.
[51] S. Baunack, S. Oswald, D. Scharnweber, Surf. Interface Anal. 26 (1998) 471.
[52] J.A. Dean, Lange's Handbook of Chemistry, 15th ed., McGraw-Hill, New York, 1999
[53] R.Y. Zheng, L. Lin, J.L. Xie, Y.X. Zhu, Y.C. Xie, J. Phys. Chem. C 112 (2008) 15502.
[54] S. Sakthivel, M. Janczarek, H. Kisch, J. Phys. Chem. B 108 (2004) 19384.
[55] L. Körösi, I. Dékány, Colloids Surf. A 280 (2006) 146.
[56] K. Yang, Y. Dai, B. Huang, J. Phys. Chem. C 111 (2007) 18985.
[57] A.M. Czoska, S. Livraghi, M. Chiesa, E. Giamello, S. Agnoli, G. Granozzi, E. Finazzi, C. Di Valentin, G. Pacchioni, J. Phys. Chem. C 112 (2008) 8951.
[58] J.C. Yu, J. Yu, W. Ho, Z. Jiang, L. Zhang, Chem. Mater. 14 (2002) 3808.
[59] X. Fan, T. Yu, Y. Wang, J. Zheng, L. Gao, Z. Li, J. Ye, Z. Zou, Appl. Surf. Sci. 254 (2008) 5191.